Electronic Supplementary Material (ESI) for Journal of Materials Chemistry A.

Supporting materials

Modulating tunable interfacial charge transfer via Z-scheme TiO_2/CdS with Ti-S bond for enhanced glucose photoreforming

Malin Eqi,[1,a,b] Cai Shi,[1,a,b] Miao Zhang,[a,b] Fuyan Kang,[a,b] Jianhua Ma,[c] Zhanhua Huang,[a,b*] Shouxin Liu[a,b]

[a] Key Laboratory of Bio-based Material Science & Technology, Material Science and Engineering College, Northeast Forestry University, Harbin 150040, China

[b] Engineering Research Center of Advanced Wooden Materials, Ministry of Education, Northeast Forestry University, Harbin 150040, China

[c] Material Science and Engineering College, Northeast Forestry University, Harbin 150000, China

1 Malin Eqi and Cai Shi contributed equally to this work

*To whom correspondence can be made

E-mail: huangzh1975@163.com (Z. Huang)

Materials

All the analytical grade materials were employed directly without further purification. Cadmium acetate ($Cd(CH_3COO)_2$) and thiourea (CH_4N_2S) were obtained from Tianjin Guangfu Fine Chemical Research Institute. Ethylenediamine, tetrabutyl titanate ($C_{16}H_{36}O_4Ti$), and hydrofluoric acid (HF) were bought from Shanghai Macklin biochemical technology Co. LTD. Acetonitrile (CH_3CN) was bought from Tianjin Xinbote Chemical Industry Co, Ltd. D-(+)-Glucose ($C_6H_{12}O_6$, AR) and ethylenediamine were purchased from Aladdin Reagent Company, China. Sodium hydroxide (NaOH) and ethanol were purchased from Tianjin Tianli Chemical Reagent Co. Deionized water was used throughout the process.

Characterization

The morphology and microstructure were acquired through Quanta200 transmission electron microscopy (TEM) and field emission scanning electron microscopy (FESEM). The XRD-6100 powder X-ray diffraction (pXRD) was carried out to obtain the crystalline and phase information. The pore size distribution and specific surface area were characterized by ASAP2020 Brunauer-Emmett-Teller (BET) method. IS10 fourier transform infrared spectroscopy (FTIR) were utilized to acquire chemical structures. The surface elemental compositions and chemical states were characterized by PHI5700 X-ray photoelectron spectroscopy (XPS) with on-monochromatic Al X-rays as the primary excitation. TU-1900 UV-vis diffuse reflectance spectrometer (UV-vis DRS) was carried out to examine light absorption property. The recombination of e^--h^+ was surveyed by G9800A photoluminescence

(PL) spectra. Radicals capture were conducted by JES electron spin resonance (ESR) with 2, 2, 6, 6-tetramethylpiperidine (TEMP), 5, 5′-dimethyl-1-pyrroline N-oxide (DMPO).

Photoelectrochemical test

All the photoelectrochemical and electrochemical measurements were carried out on CHI660E electrochemical workstation (Shanghai, China) with a three-electrode system. The three-electrode included working electrode, reference electrode (Ag/AgCl), and counter electrode (Pt plate). Na_2SO_4 solution（0.50 mol L^{-1}）was chosen as electrolyte. The working electrode was fabricated by the following detailed steps: 2 mg sample was dispersed into 1 mL ethanol with ultrasonic for 0.5 h. Then, 10 μL N-methyl-2-pyrrolidone was added to the mixed solution and settled for 5 min. Applying the mixed solution evenly on the conductive side of the Fluorine-doped tin oxide (FTO) collector, and then dried under an infrared lamp.

Photocatalytic activity test

25 mg catalyst was dispersed into 50 mL solution (25 mL deionized water and 25 mL CH_3CN) involving 1 g L^{-1} glucose and 1.5 M NaOH. Prior to exerting light, the suspension was degassed for 30 min to thoroughly exclude the dispersed oxygen in suspension to ensure the reactor was under an anaerobic state. The system was conducted under Hxuv300 Visref 300 W Xenon lamp (Beijing CEJ Tech. Co., Ltd., Beijing, China) with magnetically stirring. And the reaction system temperature was kept at 279 K by circulating condensing system. The produced H_2 was gathered H_2

was intermittently and automatically measured by gas chromatography (GC-7920, Beijing CEJ Tech. Co., Ltd., Beijing, China) with a thermal conductive detector (TCD). The liquid product were analyzed by high-performance liquid chromatography (HPLC, Agilent 1290 Infinity Ⅱ) with Hi-Plex H (300 × 7.7 mm) and Agilent Infinity Lab Poroshell 120 HILIC-Z (2.1 mm × 50 mm × 2.7 μm) columns.

DFT calculations

First-principles calculations were carried out on the basis of periodic Density functional theory (DFT) calculations using a generalized gradient approximation within the Perdew-Burke-Ernzerhof exchange correction functional. The wave functions were constructed from the expansion of plane waves with an energy cutoff of 500 eV. Gamma centered k-piont of 3×3×1 have been used for geometry optimization. The consistence tolerances for the geometry optimization are set as 1.0 $\times 10^{-5}$ eV/atom for total energy and 0.05 eV/Å for force, respectively. In order to avoid the interaction between the two surfaces, a large vacuum gap of 15 Å has been selected in the periodically repeated slabs. The top 4 atom layers have been set free. The adsorption energy was calculated according to the standard formula:

$$E_{ads} = E_{Total} - E_{TiO2} - E_{atom}$$

pXRD analysis: powder X-ray diffraction (pXRD) was carried out to further investigate the crystalline and phase information of photocatalysts (Fig. 2a). CdS exhibits distinct diffraction angles at 2θ = 26.7°, 30.5°, 43.7°, 48.3°, and 51.5°, which can be indexed to the (211), (101), (102), (110), and (103) lattice planes of CdS (JCPDS:89-1084), respectively. The pXRD spectrum of TiO_2 with diffraction peaks at 2θ = 25.1°, 37.6°, 47.9°, 53.5°, 54.9°, 62.2°, 68.7°, 70.1° and 76.0°, corresponding to the crystallographic planes (101), (001), (200), (105), (211), (213), (116), (220) and (301) of anatase TiO_2, respectively (JCPDS card number 21-1272) [1]. It is worth noting that the (001) peaks are broadened and the intensity of the (200) peaks are enhanced in the TiO_2 XRD patterns compared with the standard one (JCPDS card number 21-1272). This reveals that the nanosheets grow along the [200] directions and expose the (001) planes [2]. The exposed (001) crystal planes of TiO_2 have multiple active centers, which facilitate the e^--h^+ separation and ·OH production, resulting in improved photoreforming efficiency [3]. No peak shift is observed, which excludes the incorporation of CdS and TiO_2 into each other's lattice.

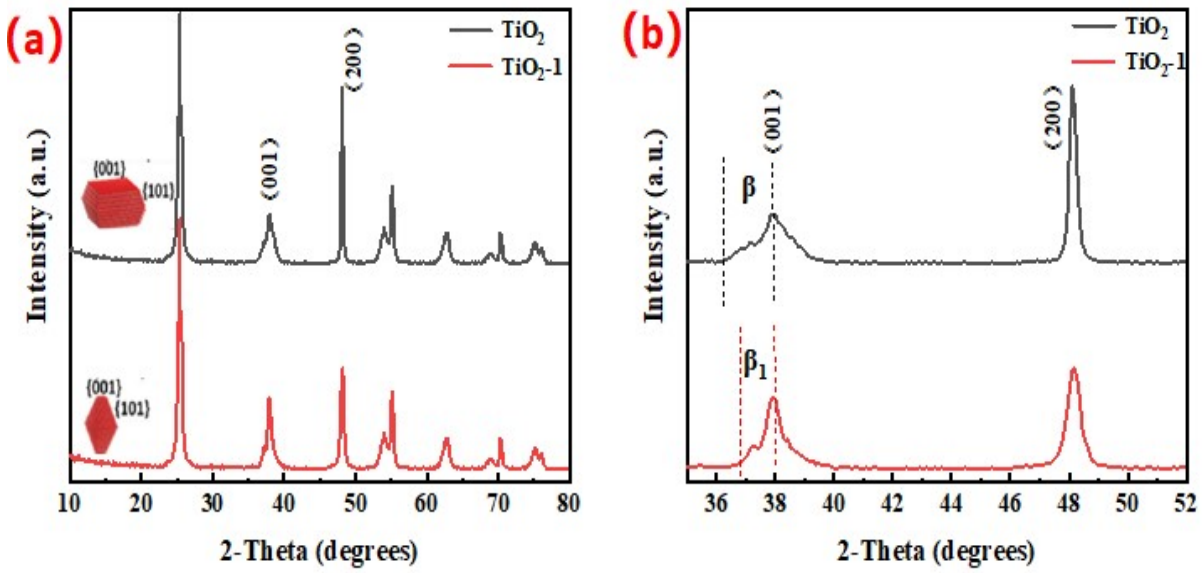

Fig. S1 (a) The XRD pattern of TiO_2 and TiO_2-1. (b) The locally enlarged XRD pattern for the (001) and (200) peaks

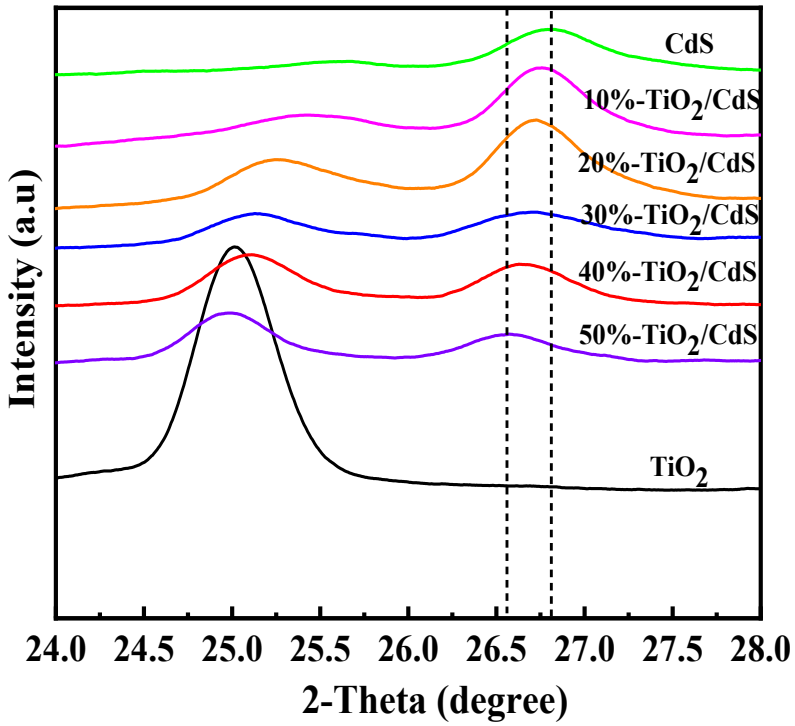

Fig. S2 The locally enlarged XRD pattern for the catalysts in the range of 24 to 28 °.

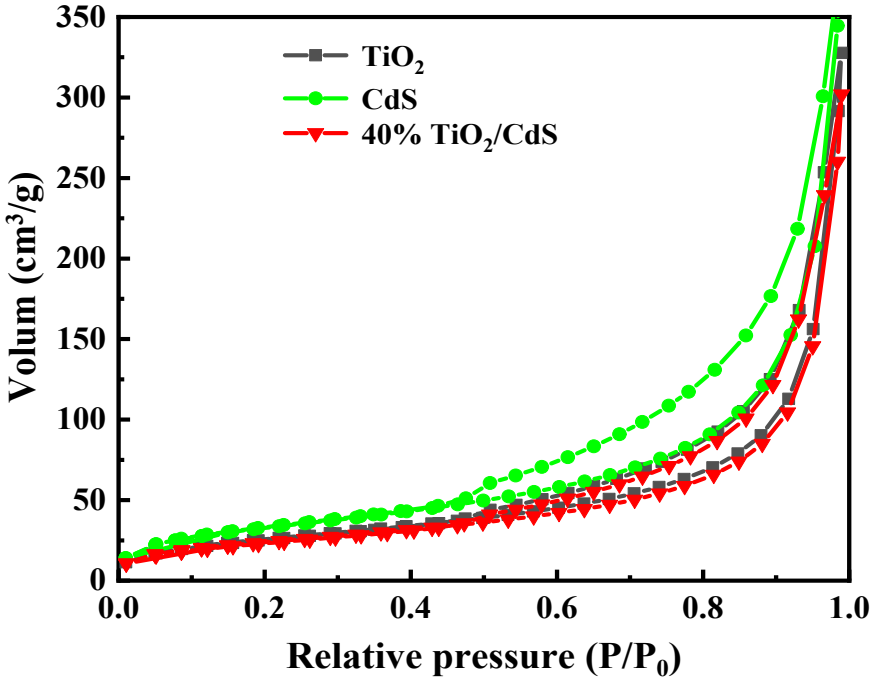

Fig. S3 The Nitrogen adsorption isotherms patterns of catalysts

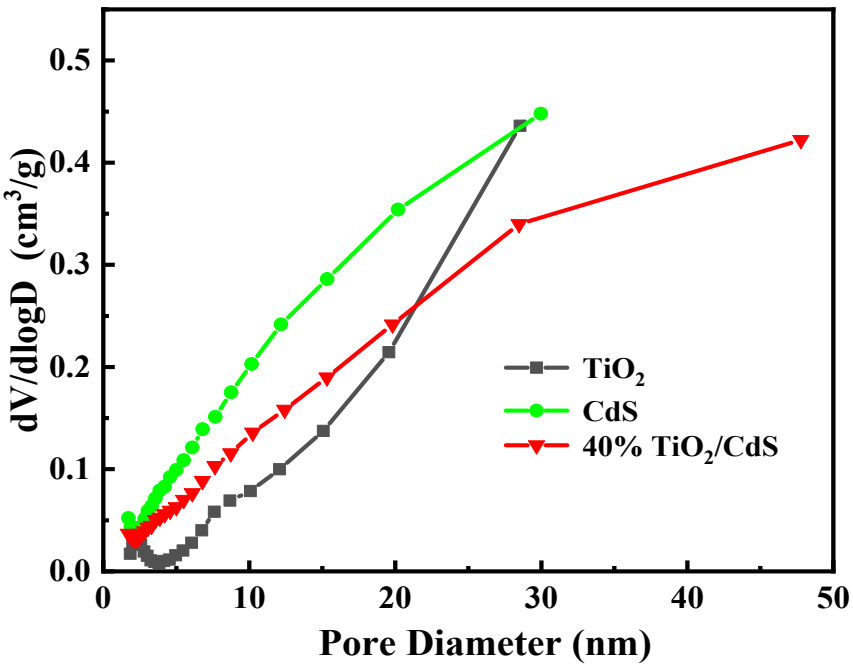

Fig. S4 The pore size distribution of catalysts

BET surface and pore size analysis: To comprehend the physical structure of TiO_2, 40%-TiO_2/CdS and CdS, N_2 adsorption–desorption isotherms, Brunauer–Emmett–

Teller (BET) surface areas model and BJH pore size distributions were acquired. As displays in (Figs. 1m and S1), the classic type IV curves with H3-type hysteresis are represented by TiO_2, 40%-TiO_2/CdS and CdS, the corresponding pore size varies from 2 to 50 nm [1]. The BET of 40%-TiO_2/CdS is marginally smaller than that of CdS, which may be attributed to the TiO_2 ultrathin nanosheets firmly anchoring on the surface of CdS via Ti-S bonds.

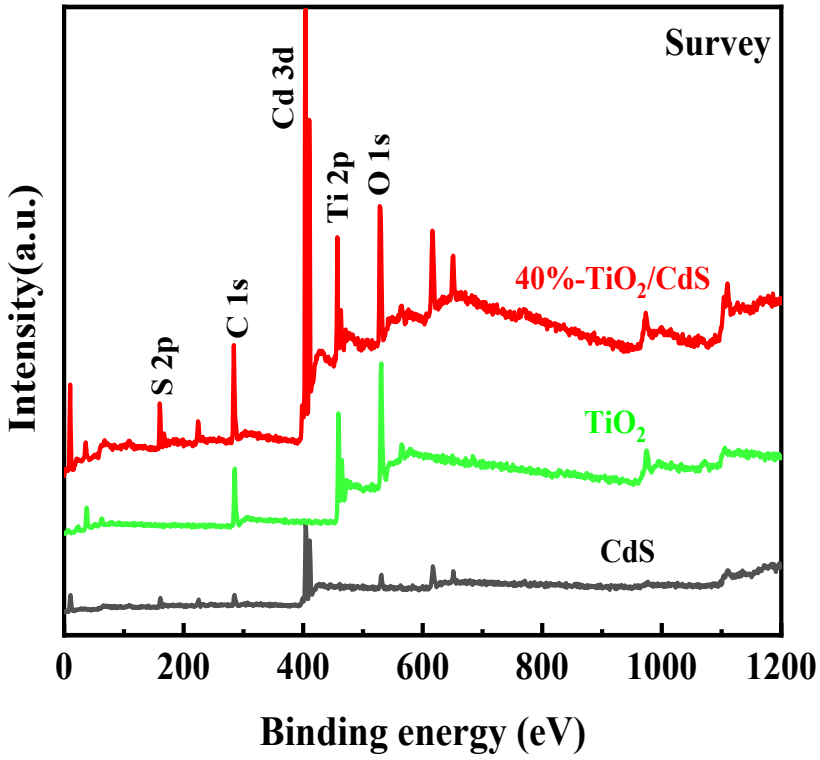

Fig. S5 The XPS survey patterns of catalyst

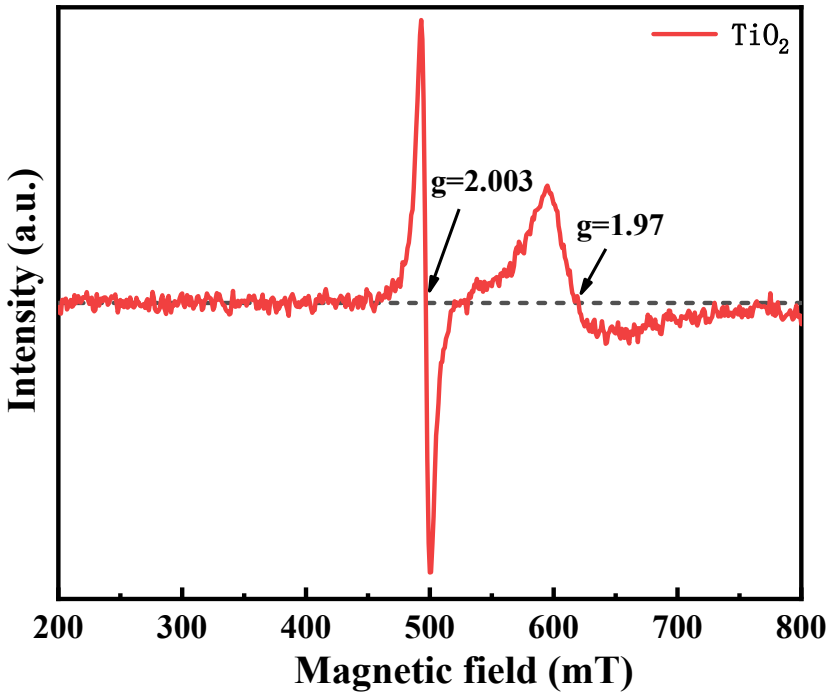

Fig. S6 The ESR spectrogram of the TiO_2 at lower temperature.

The Ti^{3+} ions are characterized by very short relaxation time, so their ESR resonances only can be detected at very low temperature, as the recombination rate of electron–hole is significantly reduced at low temperature.

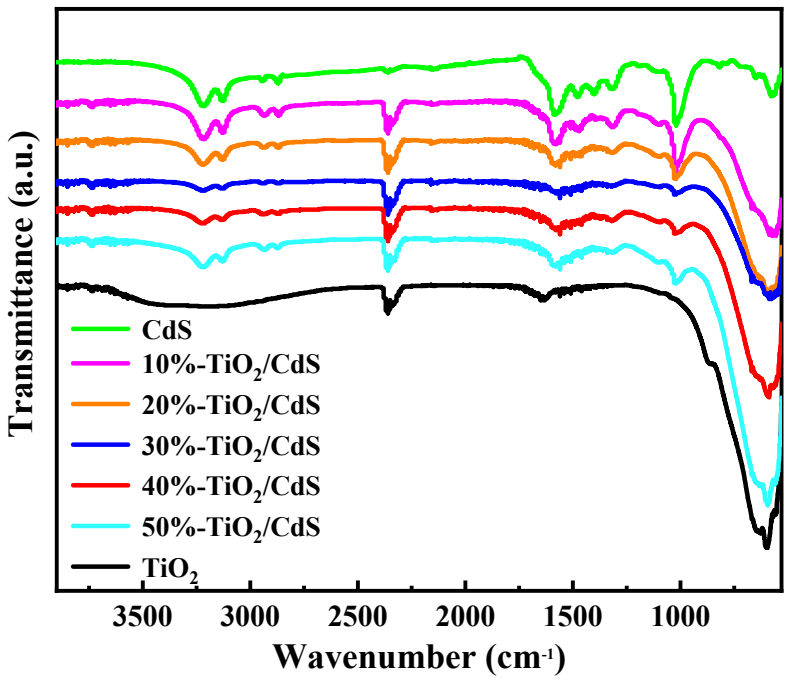

Fig. S7 The FT-IR patterns of catalysts

FT-IR analysis: As shown in Fig. S4 Fourier transform infrared spectroscopy (FTIR) was utilized to acquire chemical structures of various photocatalysts. The absorption peaks of TiO_2 at 3400 and 1631 cm^{-1} are ascribed to the ·OH stretching vibration of airborne water and the O-H bending vibration of adsorbed water molecules on TiO_2 surface, respectively [4]. The peaks at 2300-2400 cm^{-1} are related to the asymmetric stretching vibration of the C=O bond of TiO_2 [5]. The peaks near 590 cm^{-1} of the TiO_2 sample are caused by the transverse optical vibration of the Ti-O bonds, which are related to the longitudinal optical vibration represented by the broad peak of TiO_2 in the range of 700-950 cm^{-1} [6]. The peaks of CdS near 600 cm^{-1} are resulted from Cd-S stretching [7]. The peaks appear near 600 cm^{-1} and 1000 cm^{-1}, which are triggered by the Cd-S stretching and S-O bond stretching vibrations in CdS, respectively [8]. Ti-S absorption band around at 1000 cm^{-1} overlap with CdS and cannot be differentiated [9, 10]. FT-IR spectra showed peaks at 590, 1000, 1600, 2400, and 3400 cm^{-1} consistent with TiO_2 and CdS, confirming the successful fabrication of TiO_2/CdS.

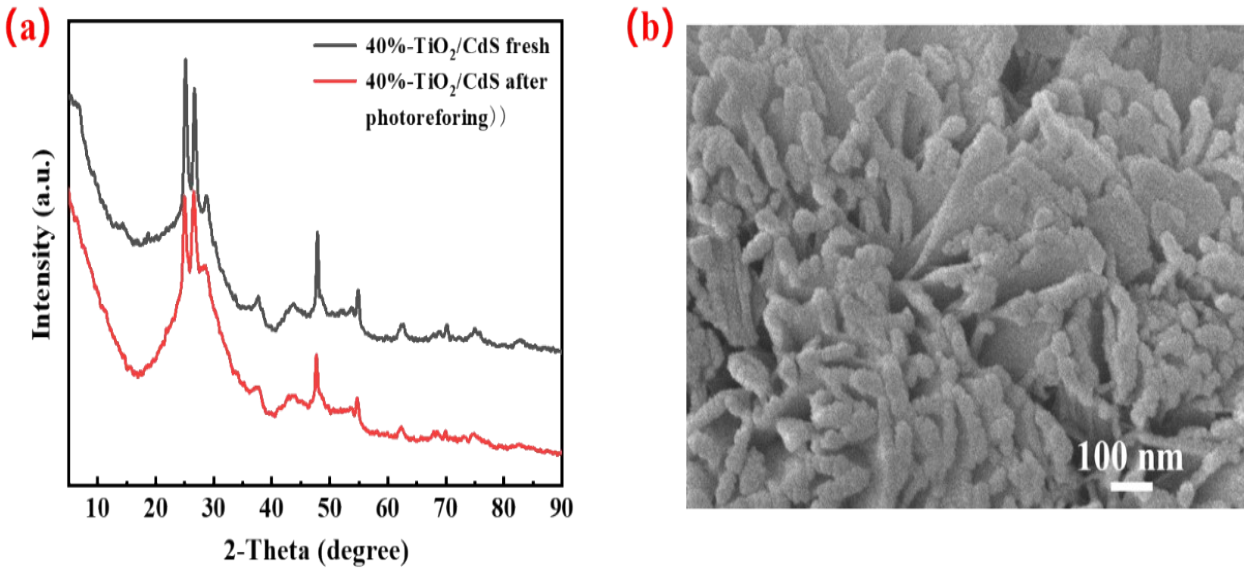

Fig. S8 (a) XRD of 40%-TiO_2/CdS fresh and after photoreforming. (b) SEM of 40%-TiO_2/CdS after photoreforming

Table S1 The effects of different catalysts on the acetic acid selectivity (%) from different biomass-based monosaccharides with various conditions

Photocatalyst	Co-catalyst	Sacrificial regent	Light souroce	Reaction temperature (℃)	HER rate (μmol h^{-1} g^{-1})	Acetic acid selectivity (%)	Ref.
$NiTiO_3$	Pt	Glucose	300W Xe	Room temperature	--	17	11
P@CN-SO_3H	None	Xylose	Sunlight	60	--	～20	12
Ut-OCN	None	Fructose	Sunlight	50	--	～5	13
CC_1@mCN_{10}	None	Xylose	Sunlight	40	--	～10	14
O-g-C_3N_4	Pt	Glucose	Sunlight	Room temperature	2500	--	15
CQDs/TiO_2	None	Glucose	300 W Xe	--	360	--	16
Pt-TiO_2-$W_{0.25}$	None	Glucose	150 W halogen lamp	--	1000	--	17

TiO_2/CdS	**None**	**Glucose**	**300W Xe**	**7**	**7080**	**74.58**	**This work**

References:

1 X. Yu, X. Fan, L. An, G. Liu, Z. Li, J. Liu, P. Hu, *Carbon*, 2018, **128**, 21-30.

2 G. Sadanandam, X. Luo, X. Chen, Y. Bao, K. P. Homewood, Y. Gao, *Appl. Surf. Sci.*, 2021, **541**, 148687-148696.

3 Y. Liu, A. Tang, Q. Zhang, Y. Yin, *J. Am. Chem. Soc.*, 2015, **137**, 11327-11339.

4 Z. Liu, Z. Jian, J. Fang, X. Xu, X. Zhu, S. Wu, *Int. J. Photoenergy*, 2012, **2012**, 1-8.

5 E. B. Aydin, G. Sığircik, H. A. M. Takci, *J. Mol. Struct.*, 2021, **1240**, 130569-130581

6 S. S. Mali, S. K. Desai, D. S. Dalavi, C. A. Betty, P. N. Bhosale, P. S. Patil, *Photoch. Photobio. Sci.*, 2011, **10**, 1652-1658.

7 Y. Li, R. He, P. Han, B. Hou, S. Peng, C. Ouyang, *Appl. Catal. B-Environ.*, 2020, **279**, 119379-119387.

8 M. B. Askari, Z. T. Banizi, S. Soltani, M. Seifi, *Optik*, 2018, **157**, 230-239.

9 T. Zhong, R. Jiang, Y. Hou, H. Chen, L. Ding, C. Lian, and B. Zou, *RRL Solar*, 2021, **6**, 2100863-2100876.

10 G. Yang, H. Shi, M. O. Jones, T. Xiao, P. P. Edwards, Z. Yan, *Appl. Catal. B Environ.*, 2010, **96**, 458-465.

11 J. Ma, D. Jin, X. Yang, S. Sun, J. Zhou, R. Sun, *Green Chem.*, 2021, **23**, 4150-4160.

12 U. Nwosu, H. Zhao, M. Kibria, J. Hu, *ACS Sustain Chem. Eng.*, 2022, **10**, 5867-5874.

13 J. Ma, D. Jin, Y. Li, D. Xiao, G. Jiao, Q. Liu, Y. Guo, L. Xiao, X. Chen, X. Li, J. Zhou, R. Sun, *Appl. Catal. B Environ.*, 2021, **283**, 119520-119533.

14 J. Ma, Y. Li, D. Jin, X. Yang, G. Jiao, K. Liu, S. Sun, J. Zhou, R. Sun, *Appl. Catal. B-Environ.*, 2021, **299**, 120698-120710.

15 A. Speltini, A. Scalabrini, F. Maraschi, M. Sturini, A. Pisanu, L. Malavasi, A. Profumo, *Int. J. Hydrogen Energ.*, 2018, **43**, 14925-14933.

16 H. Zhao, X. Yu, C. F. Li, W. Yu, A. Wang, Z. Y. Hu, S. Larter, Y. Li, M. Golam Kibria, J. Hu, *J. Energ. Chem.*, 2022, **64**, 201-208.

17 M. Bellardita, E. I. García-López, G. Marcì, G. Nasillo, L. Palmisano, *Eur. J. Inorg. Chem.*, 2018, **2018**, 4522-4532.